IEEE Access
Multidisciplinary | Rapid Review | Open Access Journal

Received February 25, 2021, accepted March 5, 2021, date of publication March 23, 2021, date of current version April 12, 2021.

Digital Object Identifier 10.1109/ACCESS.2021.3068151

Broadband Dual-Polarized Endfire Array With Compact Magneto-Electric Planar Yagi Antenna for mm-Wave Terminals

XUE-XIA YANG[1,2], (Senior Member, IEEE), NING-JIE XIE[1], NAI-DA ZHU[3], GUO-QIANG HE[1], MEILING LI[1], (Member, IEEE), AND STEVEN GAO[4], (Fellow, IEEE)

[1]School of Communication and Information Engineering, Shanghai University, Shanghai 200444, China
[2]Key Laboratory of Specialty Fiber Optics and Optical Access Networks, Shanghai University, Shanghai 200444, China
[3]Huawei Technologies Company Ltd., Shanghai 200122, China
[4]School of Engineering and Digital Arts, University of Kent, Canterbury CT2 7NZ, U.K.

Corresponding author: Xue-Xia Yang (yang.xx@shu.edu.cn)

This work was supported in part by the National Natural Science Foundation of China under Grant 61771300, and in part by Foundations of Huawei Technologies Company Ltd.

ABSTRACT Based on a newly proposed planar Yagi antenna with magnetic and electric dipoles, a compact 1×4 broadband dual-polarized (DP) array with endfire radiation is designed in this paper. The magnetic Yagi antenna operates on the vertical polarization while the electric one operates on the horizontal one. The compact configuration of $0.5\ \lambda_0 \times 0.63\ \lambda_0 \times 0.09\ \lambda_0$ benefits from the novel half-mode magnetic Yagi antenna and the arrangement with the electric Yagi antenna. The broadband characteristic comes from the directors of the magnetic and electric Yagi antennas and the reflector of magnetic Yagi antenna. The simulation and the measurement verify this design. The measured common bandwidth of $|S_{11}| < -10$ dB for both polarization ports is 23.8-30.1 GHz (23.7%), and the gains vary between 3 dBi and 4 dBi within 24.2-30 GHz band range. The 1×4 DP array with $0.5\ \lambda_0$ element space has the beam scanning range of $\pm 43^\circ$ at the endfire direction and the gain of higher than 7.1 dBi. The scanning performances are experimentally validated by two phase-shift feed networks for 0° and 30° main beam directions. The proposed endfire DP array has the good features of compact structure, a low profile and no clearance requirement, which is easy to integrate in 5G terminals.

INDEX TERMS 5G mobile communications, millimeter wave, endfire antenna array, dual polarization, half-mode, phased arrays.

I. INTRODUCTION

To meet the requirements of the high data rate and large capacity in the fifth and Sixth generation (5G/6G) mobile communication, the operation frequency of wireless communications has been extended to the millimeter wave (mm-wave) band. To compensate the losses of the mm-wave in the atmosphere, the high gain with beam scanning antenna arrays are required [1]–[3]. Dual polarized antenna could receive any polarized electromagnetic waves which is preferable for terminals. To ensure high data throughput and cover different communication standards, the antennas should operate on broadband. Thus, beam scanning array antenna with high gain, dual-polarization and broadband operations are necessary for the terminals of the next mobile communications. Some dual-polarized millimeter wave arrays with broadside radiation have been suggested for 5G/6G communications [4], [5].

The endfire antennas, having the maximum radiation direction parallel to the antenna array, are more suitable for mobile terminals [6], [7]. Endfire antennas, such as printed dipole [8]–[11], bow tie patch [12]–[14], and Vivaldi antenna [15], [16], operate on the horizontal polarization sense and have wide operation bandwidths. In order to achieve vertical polarization, these antennas need to be placed vertically [17]. As a result, the profiles of those dual-polarized (DP) endfire antennas were high and they are not practical.

The associate editor coordinating the review of this manuscript and approving it for publication was Tutku Karacolak.

TABLE 1. Performance comparison with other published endfire antennas.

Ref.	Antenna type	Polarization	Array	Band(GHz)	Element Gain(dBi)	thickness(λ_0)	size($\lambda_0\times\lambda_0$)	clearance(λ_0)
[8]	Printed dipole	HP	1×8	26.5-38.5 (36.2%)	4.5-5.8	0.02	0.51×0.55	0.51
[15]	Vivaldi antenna	HP	1×8	24.55–28.5 (14.9%)	Not given	0.08	1.18×0.5	0.5
[19]	Quasi-Yagi antenna	DP	1×4	35.6-38.3 (7.3%)	6.5-8	0.24	0.91×1.54	1.35
[20]	Dipole & SIW horn	DP	1×4	27.5-29.5 (5.3%)	3.88-6.7	0.1	0.56×2.04	0.25
[23]	H-pol and V-pol dipoles	DP	1×3	28-33GHz (23%)	Not given	0.35	0.5×2	0.28
[30]	Microstrip MD	VP	\	4.87-5.55 (13.1%)	4-6	0.08	1.90×2.08	0
This work	Yagi ME	DP	1×4	23.8 -30.1 (23.7%)	3.8-5.2	0.09	0.5×0.63	0

The monopole, with a length of half a dipole, can reduce the profile of the vertical polarized antenna effectively. The DP endfire antenna had a profile of 0.11 λ_0 (λ_0 is the wavelength of the electromagnetic wave in the air) by using an upright monopole and a printed Yagi dipole in [18]. The overlapped 10-dB impedance bandwidth was from 37.5 to 42 GHz (12.5%). In [19], Hsu loaded a director in front of the driven monopole and the gain was enhanced to 7.3 dBi. However, the profile was increased to 0.24 λ_0. In [20], Hong designed a quasi-Yagi DP antenna by utilizing the magnetic and electric dipoles. The total height was about 0.07 λ_0, while the overlapped 10-dB impedance bandwidth was only from 27.1 to 28.1 GHz (3%). Some efforts have been proposed for extending the bandwidth. The designed mm-wave DP arrays in [21], [22] and [23] had the 10-dB impedance bandwidth of 5.3%, 8.3%, and 14%, respectively. To keep the antenna performances from being affected by the metal frame, the aforementioned DP endfire antennas in [18]–[23] need the clearance when they are placed in the terminals.

Microstrip magnetic dipole (MMD) had low profile and could excite V-pol waves in the endfire direction [24]–[28]. The full metal ground at the bottom makes it easy for integration. In [29], Wen designed a MMD antenna with bidirectional radiation at the endfire directions. However, the bandwidth was only about 3%. In [30], the bandwidth of the MMD was broadened to 13.1% by using microstrip patch, while the element size was too large (1.90 λ_0 × 2.08 λ_0) to suitable for array design.

Based on the half-mode theory, this paper proposes a novel magnetic Yagi antenna, which has wide operation band and endfire radiation characteristic. Combining this magnetic Yagi antenna with a planar electric Yagi antenna, a compact wideband DP antenna with endfire radiation is suggested. Taking the element space as 0.5 λ_0, the 1 × 4 antenna array is designed and verified by the measurements. A DP beam coverage of ± 43 ° in the endfire direction is obtained with phase control. The overlapped 10-dB impedance band covers the 5G bands of n257 and n258. The bottom of the proposed DP antenna is complete metal ground, so no clearance is required, which make it easy to integrate the DP antenna with chips by the printed circuit board (PCB) technology.

In this paper we presented a DP endfire antenna and Table 1 compares the proposed antenna with those in the published papers. The operation band in the table is the overlapped impedance bandwidths of $|S_{11}|$ and $|S_{22}|$ less than −10 dB of two polarizations. Compared with other DP antenna, this design has a lower profile and a wider bandwidth of 23.7%. The antenna size is only 0.5 λ_0 × 0.63 λ_0 × 0.09 λ_0, which is the smallest one among other dual-polarized antennas. Furthermore, the bottom of the antenna is full metal structure, so no clearance will be required. This antenna will be easy to integrate to the chips of 5/6G mobile terminals.

The rest of this paper is organized as follows. Section II illustrates the structure and the operation principle of the newly proposed planar half-mode magnetic Yagi antenna. Section III presents the configuration, performances and experimental verification of the broadband DP endfire Yagi antenna composed of the magnetic and electric dipoles. The simulation and measurement of the 1 × 4 dual polarized endfire antenna array with beam scanning are addressed in Section IV. Finally, conclusions are drawn in Section V.

II. PLANAR HALF-MODE MAGNETIC YAGI ANTENNA

In order to investigate the operation principle of the novel planar half-mode magnetic Yagi (HMMY) antenna, the evolution process of four antenna prototypes is analyzed. They are the microstrip magnetic dipole (MD), the reflector-loaded MD, the magnetic Yagi (MY) antenna, and the HMMY antenna, as drawn in Fig. 1. It should be noticed that the metallic walls are set as the ideal metal in the HFSS simulation while they are realized by metallic vias of SIW in PCB for fabrication.

The MD antenna is printed on one layer substrate and the structure is shown in Fig. 1 (a). It consists of one patch on the top plane, three shorted metal walls, and a feed probe. Five metal boundaries surround a cavity, while the open aperture radiates the vertical polarized wave (relative to the aperture) to the endfire direction, which is in x direction. This open aperture can be considered as a ‘‘magnetic

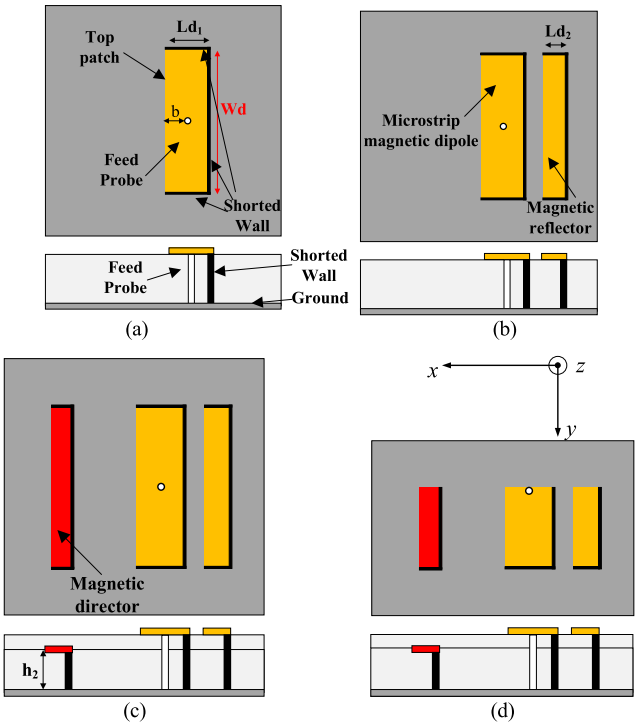

FIGURE 1. Four prototypes of the microstrip magnetic antennas. (a) MD. (b) Reflector-loaded MD. (c) MY antenna. (d) HMMY antenna.

dipole" (MD). The length Ld_1 and the width Wd of the top patch determine its operation frequency. This magnetic dipole is fed by a probe from the bottom of the dielectric substrate to the top patch. By shifting the position b of the probe from the open aperture, the input impedance could be matched. The HFSS software is used to simulate and analyze the antenna performances. The simulated $|S_{11}|$ versus frequency of the magnetic dipole is plotted as the solid line in Fig. 2. It can be found that $|S_{11}| < -10$ dB is from 26.2 to 29.4 GHz (11.5%).

By loading a magnetic reflector behind this driven MD, as shown in Fig.1 (b), another resonance frequency appears at the low band. This new resonance frequency is determined by length Ld_2 of the magnetic reflector. The reflection coefficients versus frequency are also shown in Fig.2. It can be seen that the low resonance frequency shifts toward lower band when Ld_2 is increased, so the bandwidth is broadened. However, $|S_{11}|$ at the low resonance frequency becomes higher and the bandwidth enhancement is not obvious with the increase of Ld_2. Considering the impedance match characteristic, Ld_2 is 0.85 mm in this design. So and the band of $|S_{11}| < -10$ dB is from 24.5 to 30 GHz (20%).

By loading a magnetic director in front of the driven one, a MY antenna is formed, which is shown in Fig.1(c). In order to reserve enough space for the electric printed dipole, the height h_2 of the magnetic director is slightly lower than the thickness h of the substrate. Fig.3 shows the simulated *xoz*- and *yoz*-plane patterns of the antenna prototypes in Fig. 1 (a), (b), and (c) at 25 GHz and 29 GHz. It can be found that the electromagnetic waves are concentrated to the endfire direction ($+x$ axis) by loading the magnetic reflector

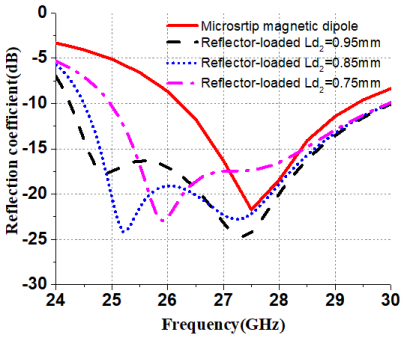

FIGURE 2. Simulated reflection coefficient of the MD and the reflector-loaded MD with different length of Ld_2.

and director, so the gain could be improved. It can also be seen that the patterns on the *xoz* plane shift away from 0 °, which is caused by the ground. However, this shift of the maximum direction will not influence the beam scanning characteristic of the phased array. The simulation results have found that the magnetic director has few impacts on the impedance match so the corresponding reflection coefficients were not given in Fig. 2.

The planar HMMY antenna is proposed by cutting half of the MY antenna along the symmetrical plane, as shown in Fig. 1(d). The antenna size is greatly reduced comparing to the full-mode one. To validate the effectiveness of the half-mode theory, the current distributions have been investigated. Fig. 4(a) plots the vector current distributions on the full-mode MY antennas. It can be seen that the vector current is completely symmetrical to the center line, which can be equivalent to a magnetic wall. A reasonable prediction can be drawn that half of the MY antenna would have the same characteristic. Fig.4 (b) draws the simulated vector current distribution on the HMMY antenna, which verifies our prediction. The HMMY antenna has the same current distribution and would have the same radiation characteristics comparing to the full-mode MY antenna. Consequentially, the width Wd of the HMMY antenna could be reduced obviously, and the miniaturization is realized.

III. BROADBAND DUAL-POLARIZED ENDFIRE YAGI ANTENNA

By combing the novel printed HMMY antenna with an electric Yagi antenna, The DP antenna is proposed. Fig. 5 shows the top, side and 3D views of the DP end-fire antenna, which is printed on two dielectric substrate layers.

It should be noticed that the two substrate layers come from the heights of the director dipole and the driven one of the MY antenna and they have the same dielectric constant. The HMMY is feed by a coaxial line at probe 1.

The printed electrical Yagi antenna is on the top plane and is composed of a balun feed network, a printed dipole and an electric director. The driven electric dipole is fed by probe 2 through the balun. The top patch of the magnetic director provides the metal ground for the balun, which makes the DP magnetic-electric Yagi antenna more compact.

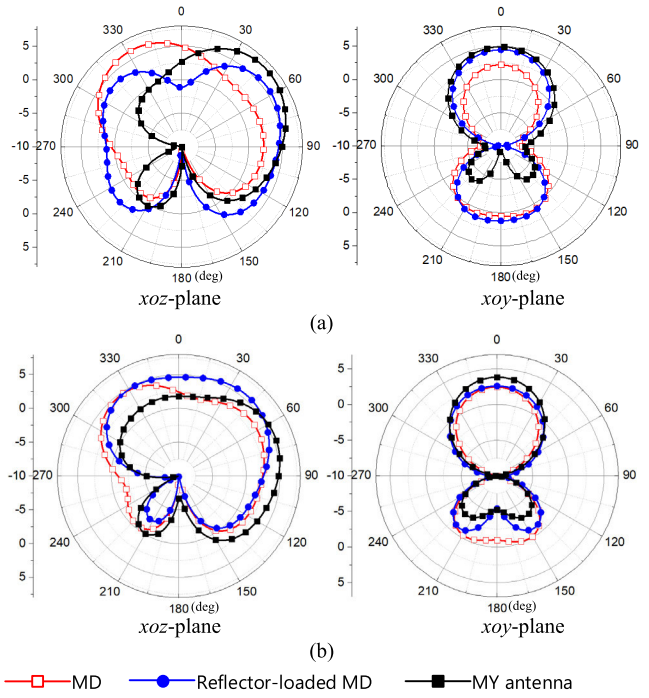

FIGURE 3. Radiation gain patterns of the antenna prototypes of MD, reflector-loaded MD and MY. (a) At 25 GHz. (b) At 29 GHz.

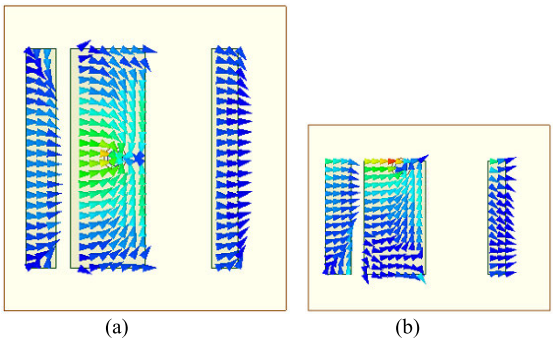

FIGURE 4. Vector current on the patches of the magnetic Yagi antenna.

Before investigating the DP antenna characteristics, the polarizations should be defined firstly. The direction of x, parallel to the ground plane, is the endfire direction. When the electric field vectors are parallel to the ground plane (xoy plane), it is named as the horizontal polarization (H-pol) wave. When the electric field vectors are perpendicular to the ground plane (xoz plane), it is called the vertical polarization (V-pol) wave. The suggested HMMY and the electrical Yagi antennas excite V- and H-pol waves, respectively.

The bottom of the DP antenna is complete ground plane, which gets the benefit of no requirement of any clearance in the practical mobile terminals. This good feature will be illustrated in following description about the electrical Yagi antenna.

The used substrate is TSM-DS3 with a relative dielectric constant of 2.92 and the loss tangent of 0.002. The total thickness is 1.027 mm ($0.09\lambda_0$), and the size is 5.5 mm $\times$ 7.0 mm ($0.5\ \lambda_0 \times 0.63\ \lambda_0$).

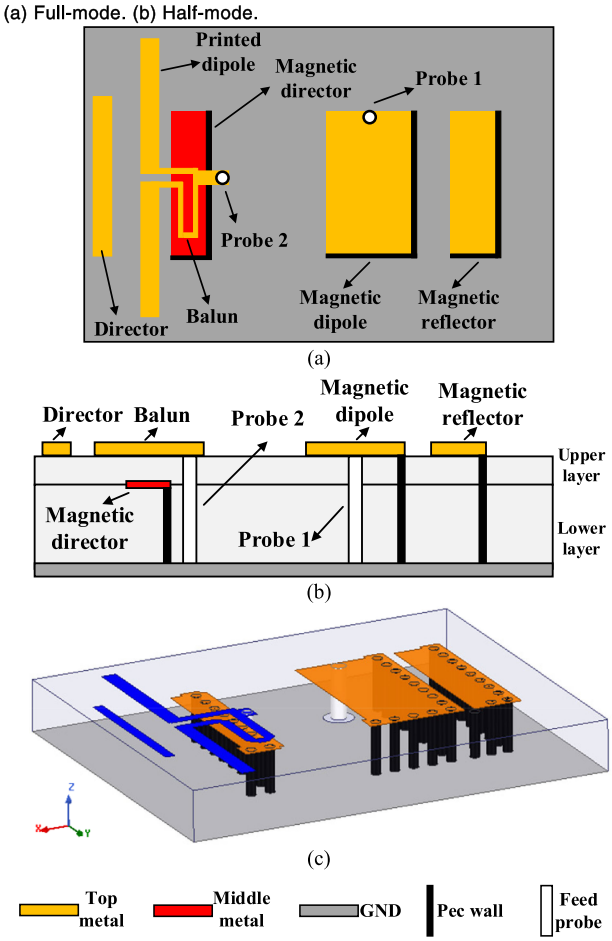

FIGURE 5. Structure of DP antenna element. (a) Top view. (b) Side view. (c) 3D view.

A. HORIZONTAL-POLARIZED PRINTED ELECTRIC YAGI ANTENNA

As shown in Fig. 6(a), the electrical Yagi antenna consists of an electric director, an electric dipole, a balun feed network, and a feed probe, and is printed on the top plane of the substrate. The bottom plane is a full metal ground. The probe feeds the electric dipole through the balun. The balun is located just above the magnetic director. The top patch of the magnetic director not only provides the metal ground for the balun but also can improve the impedance match characteristic, which makes the structure more compact. The electric director dipole can broaden the bandwidth and increase the gain.

In most instances, the covers of mobile phones and other terminals are metal, which will deteriorate the dipole characteristic so a clearance below the dipole is required. The electrical Yagi antenna with and without the clearance are shown in Fig. 6. Generally, the coupling between the electrical dipole and the ground will induce the impedance mismatch. The height between the top electric dipole and its balun is h1. The influence of the substrate thickness h on the impedance match characteristic will be investigated.

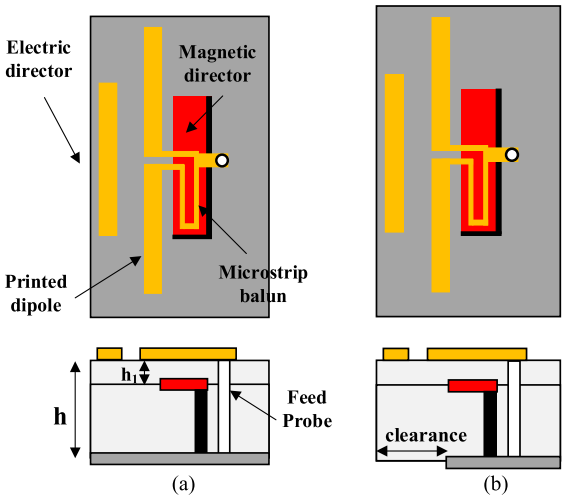

FIGURE 6. The structure of electric printed dipole. (a) with full GND. (b) with clearance.

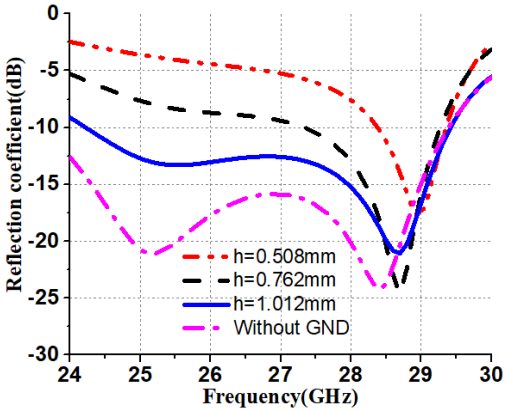

FIGURE 7. Simulated reflection coefficient of the electric printed dipole.

By keeping h_1 as 0.127 mm, the influences of height h on the reflection coefficient are plotted in Fig. 7. When h is less than 0.508 mm, the operation band of the electric dipole is very narrow. As h increases, the bandwidth becomes wider and tends to that of the electric dipole without ground, namely with clearance. In this design, h is taken as 1.012 mm for tradeoff between the antenna performance and the profile. The simulated reflection coefficient less than −10 dB is from 24.2 to 29.5 GHz. The director of the V-Pol element offers the ground to the balun of the H-Pol element, which makes the H-Pol and V-Pol element and array have compact size.

B. DUAL-POLARIZED ENDFIRE MAGNETO-ELECTRIC YAGI ANTENNA

The final configuration and the geometrical sizes of the endfire DP magnetic-electrical Yagi antenna are shown in Fig. 8. In order to make the facilitation easier, the shorted metal walls are all replaced by metallized vias. It should be noticed that there is a little difference between the metal-wall-loaded and the metal-vias-loaded DP antenna prototype.

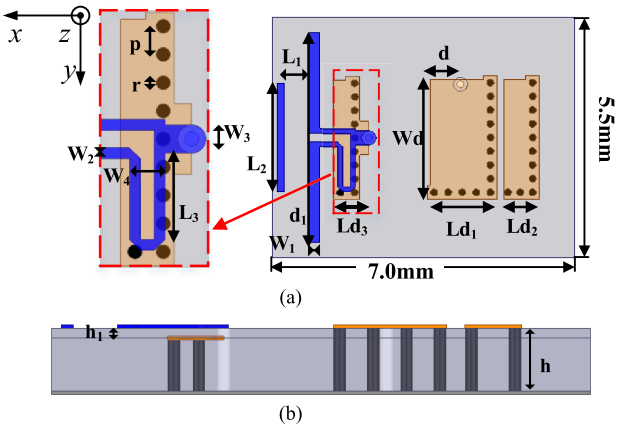

FIGURE 8. Structure of the DP endfire antenna element. (a) top view. (b) side view.

TABLE 2. Parameters of the antenna element (unit: millimeter).

L_1	L_2	L_3	Ld_1	Ld_2	Ld_3	h	h_1
5.2	3.2	1.25	1.9	1.0	0.85	1.016	0.127
W_d	W_1	W_2	W_3	W_4	d	r	p
3.4	0.3	0.2	0.4	0.6	0.85	0.2	0.4

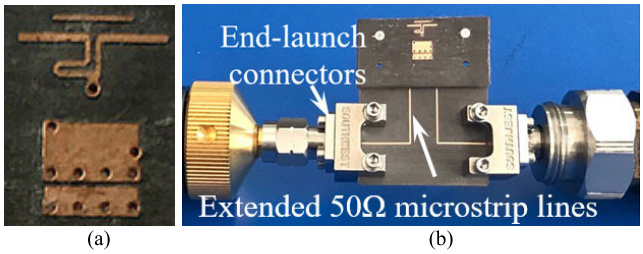

FIGURE 9. Prototype of the DP element. (a) Element. (b) Test setup.

After optimizing, the final geometric parameters are listed in Table 2.

The DP Yagi antenna is manufactured by using the PCB process. The 50 Ω microstrip line has been extended for connecting the end-launch connector for measurement. The radiations have been measured in the chamber and the S-parameters were tested by a VNA. Fig. 9 shows the fabricated sample of the DP antenna including the extended 50Ω microstrip line and the end-launch connector.

The simulated and measured S-parameters versus frequency are shown in Fig. 10. Port1 and Port2 are the feeding ports for the V-pol and H-pol waves, respectively. The simulated reflection coefficients of $|S_{11}|$ and $|S_{22}|$ less than −10 dB are from 24.25 to 30.0 GHz (21%), and 24.25 to 29.4 GHz (19.2%), respectively. Meanwhile, those of measured results are from 23.8 to 30.2 GHz (23.7%), and 23 to 30.1 GHz (26.7%), respectively. The measured isolations of $|S_{12}|$ are all greater than 21 dB within the whole operation band. It is found that the measured bandwidths of reflection coefficients are slightly wider than the

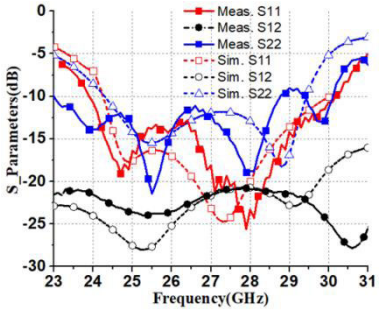

FIGURE 10. Simulated and measured S-parameters versus frequency of the DP element.

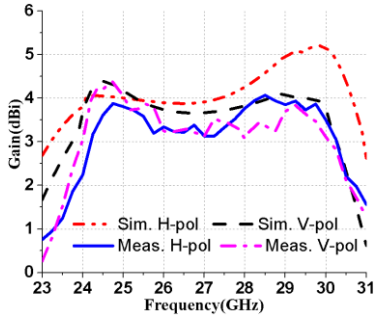

FIGURE 11. Simulated and measured Gains versus frequency of the DP element.

simulated ones and the measured isolation from 29.5 GHz to 31 GHz is higher than that of the simulated one, which was mainly caused by connecting the end-launch in the measurement processes. However, the simulation and the measurement results have good agreement within a broadband from 23.8 to 30.2 GHz.

Fig. 11 shows the gain of the DP Yagi antenna versus the frequency. The measured gains of the two polarized antenna vary between 3 dBi to 4 dBi within 24.2-30 GHz band range. The measured gains are lower than those of simulation. This may be due to the insert losses of the extended microstrip lines, the end-launch connector and solder process.

Figs.12 and 13 show the radiation patterns of the printed electric and the magnetic Yagi antennas at 26 GHz and 28 GHz, respectively. The simulated front-to-back ratios of the V-Pol are 12 dB and 13 dB at 26 GHz and 28 GHz, respectively, while those of the H-Pol are 9 dB and 7 dB, respectively. Although more director can improve the gain of the Yagi antenna, only one director has been applied in this design considering the miniaturization for the mobile terminal applications. It can be found that the simulated and the measured patterns from -90 ° to 90 ° coincide to each other well and the little difference has mainly been caused by the connectors. Due to the limitation of the chamber measurement system, -90 ° $\sim$ 90 ° forward patterns have been measured. It could be found that the measured patterns coincide with the simulated results, and the cross polarization is lower than -15 dB at the main radiation direction.

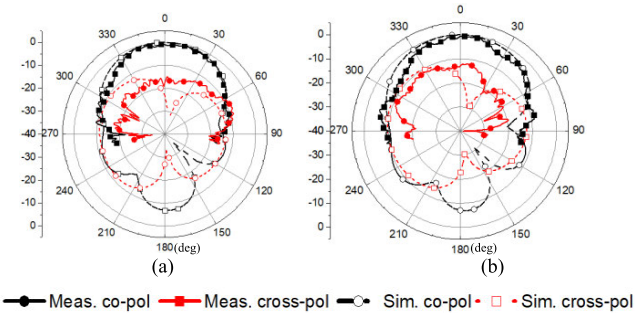

FIGURE 12. Simulated and measured radiation patterns of the H-pol in xoy-plane. (a) At 26 GHz. (b) At 28 GHz.

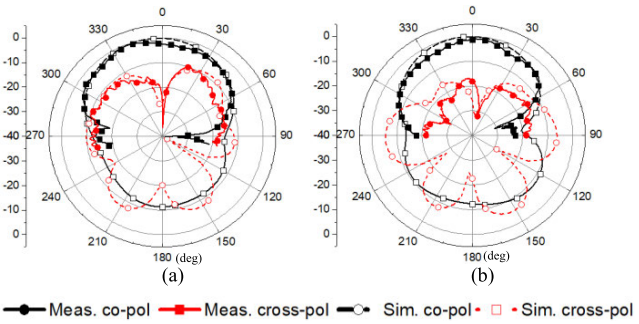

FIGURE 13. Simulated and measured radiation patterns of the V-pol in xoy-plane. (a) At 26 GHz. (b) At 28 GHz.

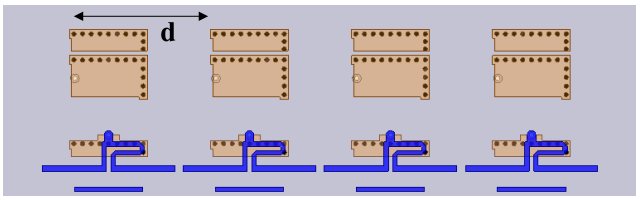

FIGURE 14. The configuration of the 1 × 4 array.

IV. 1 × 4 DUAL-POLARIZED ENDFIRE YAGI ARRAY

A dual-polarized 1 × 4 magnetic-electric Yagi array with endfire radiation is formed by using the proposed DP antenna element, which is shown in Fig. 14. Fed with appropriate phase for every element, the array can scan the beam in different directions. Due to the advantages of the miniaturized DP Yagi antenna, the space between the antenna elements can be taken as d = 0.5 λ_0 = 5.5 mm. Therefore, the side lobe level of the array can remain a low level, and a wide scanning angle range can be obtained.

A. SIMULATIONS AND ANALYSIS OF THE DP ARRAY

Fig.15 shows the simulated reflection coefficient of the DP array versus frequency. Ports 1 to 4 are the vertical polarization ports, and ports 5 to 8 are the horizontal ones. The simulated bandwidth of reflection coefficient less than -10 dB is from 24.2 to 29.5 GHz, which is similar to that of the element. Fig. 16 shows the isolation between ports 1 to 8 versus frequency. The isolations are all higher than 17 dB within the operating band.

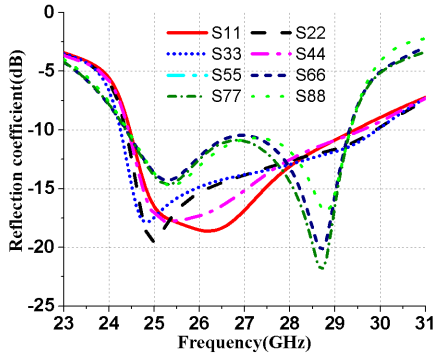

FIGURE 15. The reflection coefficient of the DP array versus frequency.

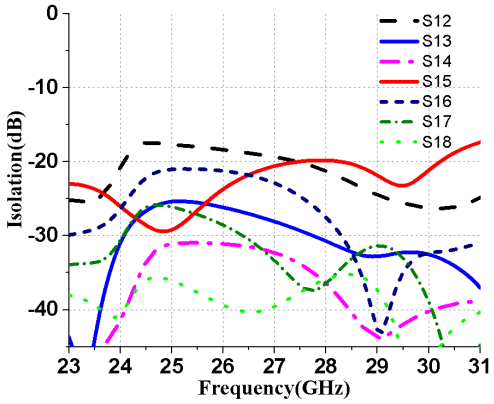

FIGURE 16. The isolation of the DP array versus frequency.

With the same amplitude and appropriate phase at each port, the beam-scanning performance at the endfire direction can be achieved. Fig. 17 plots the simulated beam-scanning performance of H-pol and V-pol waves at 26 and 28 GHz. The array yielded a scan angle up to 43 ° at both frequencies. The gains for the two polarizations at 26 and 28 GHz are 7.1/8.1 dBi and 7.8/8.7 dBi, respectively. Fig. 18 gives the simulated radiation and total efficiencies of the H-pol and V-pol array versus frequency. Within the whole operation band, the radiation and total efficiencies of the H-pol are above 91.7% and 90.7%, respectively, while those of the V-pol are above 97.7% and 89.5%, respectively.

B. BEAM SCANNING PERFORMANCE AND MEASUREMENTS OF THE DP ARRAY

In order to verify the beam scanning performance of the DP array, the T-type phase-shift feed networks are designed to excite the DP waves with the main beams at 0 ° and 30 ° directions. Fig. 19 shows the layouts and the fabricated prototypes of the DP arrays with V- and H-pol waves at 0 ° scanning angle. The T-type power divider with 4 outputs is designed to feed 4 elements in the same amplitude and phase. Fig. 20 gives out the Photograph of the fabricated prototypes of the proposed array, and Fig. 21 shows the simulated and measured reflection coefficients of V- and H-pol ports versus frequency. The

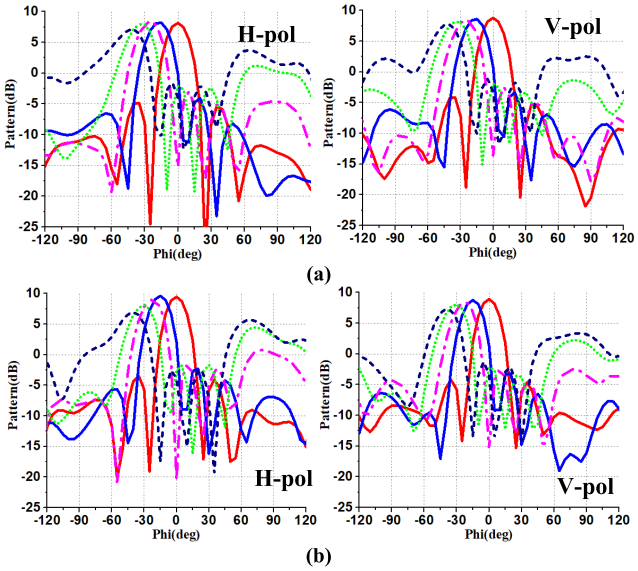

FIGURE 17. Beam-scanning performance of the DP array. (a) At 26GHz. (b) At 28GHz.

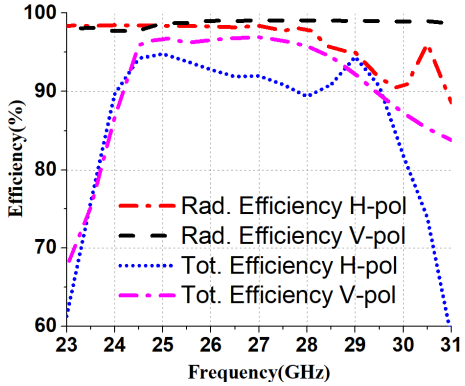

FIGURE 18. Radiation efficiency and total efficiency vs. frequency.

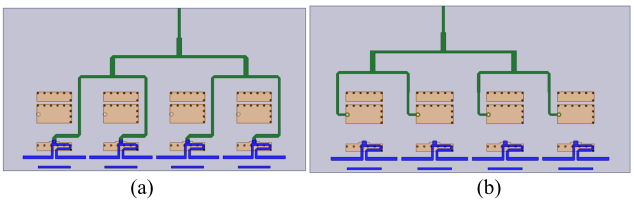

FIGURE 19. Simulated model of 0 ° scanning angle. (a) H-pol array. (b) V-pol array.

measured 10-dB impedance bandwidth of V- and H-pol ports are 24.0∼30.1 GHz and 24.7∼29.5 GHz, respectively. The measured results are slightly worse than the simulated ones, which might mainly be caused by processing errors, soldering and experiment process.

Fig. 22 shows the simulated and measured normalized patterns of H-pol and V-pol at 26 and 28 GHz. It can be seen that the measured patterns are nearly the same as the simulated ones. When the main beam is at the 0 ° direction, the measured side lobes are about −10 dB and −9 dB at

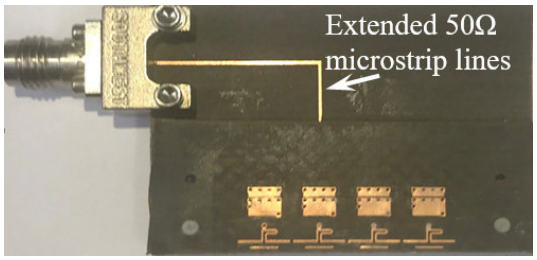

FIGURE 20. Photograph of the fabricated prototypes of the proposed array.

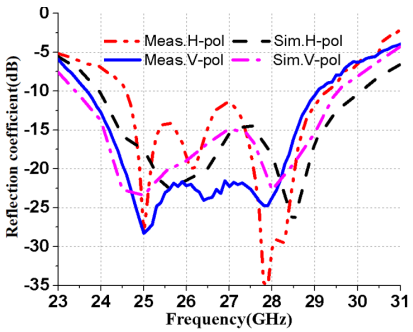

FIGURE 21. Reflection coefficient versus frequency of 0 ° scanning angle.

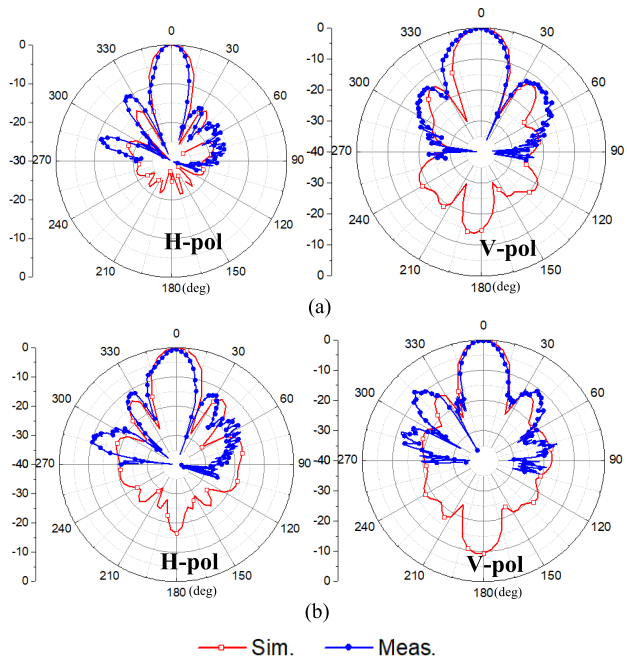

FIGURE 22. Normalized radiation pattern of the array at 0 ° scanning angle. (a) At 26 GHz. (b) At 28 GHz.

26 and 28 GHz, respectively. Fig. 23 plots cross polarization versus frequency. It can be seen that the H-Pol and V-Pol are lower than −17.4 dB and −17.5 dB at the main radiation direction, respectively. The side lobes are slightly higher than the simulated ones, which may be caused by reflections of the end-launch connector and the cables of the measurement setup.

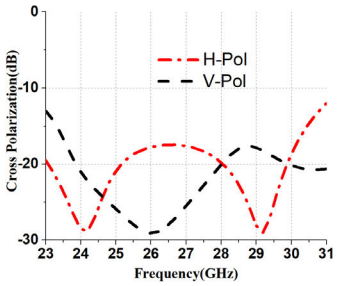

FIGURE 23. Cross polarization of array versus frequency at the main radiation direction.

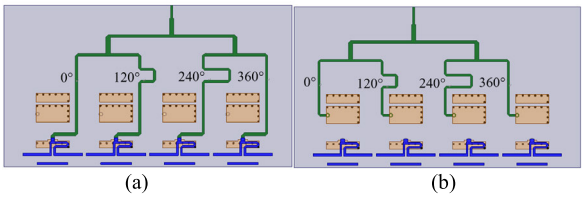

FIGURE 24. Simulated model of 30 ° scanning angle. (a)H-pol array. (b)V-pol array.

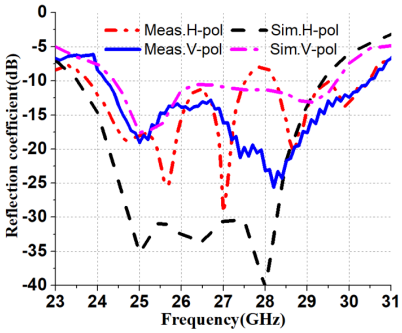

FIGURE 25. Reflection coefficient versus frequency of 30° scanning angle.

Fig. 24 shows the DP arrays with V- and H-pol waves at 30 ° scanning angle. The 4 outputs of the T-type power divider have the phase difference of 0 °, 120 °, 240 °, and 360 °, respectively. Fig. 25 shows the simulated and measured reflection coefficients of V- and H-pol versus frequency. The measured 10-dB impedance bandwidth of V- and H-pol ports are 23.8∼30.5 GHz and 24.2∼30.5 GHz, respectively. Although the measured reflection efficient are higher than the simulated ones, the trends and operation bands coincide with each other well. The higher reflection coefficient have been caused by processing errors, soldering and experimental process.

Fig. 26 plots the simulated and measured normalized patterns of H-pol and V-pol at 26 and 28 GHz. It can be seen that the measured main beams are pointed at 30 ° direction. The side lobes are −10 and −9 dB, respectively, which is same as those of the 0 ° direction. The measured pattern is nearly the same with the simulated ones except that the side lobe is slightly higher than the simulated ones.

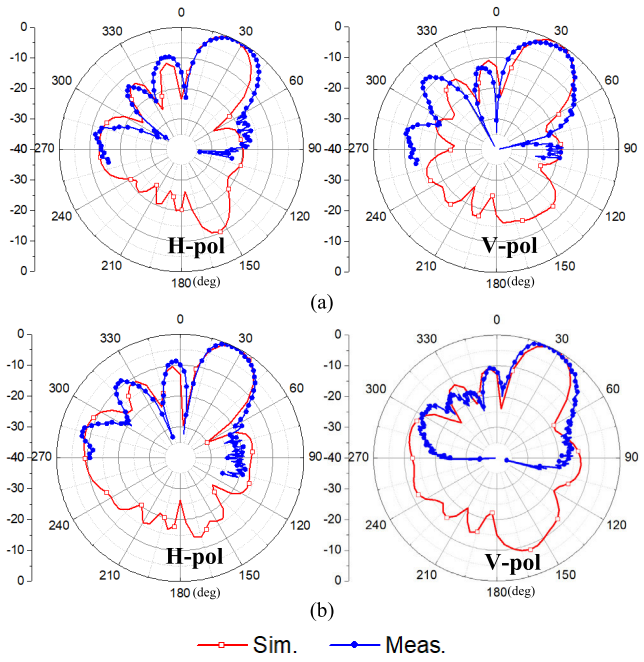

FIGURE 26. Normalized radiation pattern of the array at 30 ° scanning angle. (a)At 26 GHz. (b)At 28 GHz.

V. CONCLUSION

This paper proposed a compact Yagi magneto-electric dipole antenna with a newly suggested half-mode magnetic Yagi antenna. It operates on broadband, dual-polarization and end-fire radiation. The 10-dB impedance bandwidth covers the 5G bands of n257, n258. The size of the element is only 0.5 $\lambda_0 \times 0.63\ \lambda_0$, and the profile is only 0.09 λ_0, which is easy to design arrays. A 1 × 4 array for beam scanning is designed by using this compact DP element. This array can achieve DP beam coverage of ± 43 ° in the endfire direction with appropriate phase differences among four feed ports. Simulation and measurement results verify the design. This compact 1 × 4 array can be directly integrated with chips with no clearance requirement for 5G terminal applications.

REFERENCES

[1] Z. Pi and F. Khan, "An introduction to millimeter-wave mobile broadband systems," *IEEE Commun. Mag.*, vol. 49, no. 6, pp. 101–107, Jun. 2011.

[2] T. S. Rappaport, S. Sun, R. Mayzus, H. Zhao, Y. Azar, K. Wang, G. N. Wong, J. K. Schulz, M. Samimi, and F. Gutierrez, "Millimeter wave mobile communications for 5G cellular: It will work!," *IEEE Access*, vol. 1, pp. 335–349, 2013.

[3] X. Wang, L. Kong, F. Kong, F. Qiu, M. Xia, S. Arnon, and G. Chen, "Millimeter wave communication: A comprehensive survey," *IEEE Commun. Surveys Tuts.*, vol. 20, no. 3, pp. 1616–1653, 3rd Quart., 2018.

[4] B. Feng, L. Li, K. L. Chung, and Y. Li, "Wideband widebeam dual circularly polarized magnetoelectric dipole antenna/array with meta-columns loading for 5G and beyond," *IEEE Trans. Antennas Propag.*, vol. 69, no. 1, pp. 219–228, Jan. 2021.

[5] Q. Yang, S. Gao, Q. Luo, L. Wen, Y.-L. Ban, X. Ren, J. Wu, X. Yang, and Y. Liu, "Millimeter-wave dual-polarized differentially fed 2-D multibeam patch antenna array," *IEEE Trans. Antennas Propag.*, vol. 68, no. 10, pp. 7007–7016, Oct. 2020.

[6] J. Helander, K. Zhao, Z. Ying, and D. Sjöberg, "Performance analysis of millimeter-wave phased array antennas in cellular handsets," *IEEE Antennas Wireless Propag. Lett.*, vol. 15, pp. 504–507, 2016.

[7] K. Zhao, S. Zhang, Z. Ho, O. Zander, T. Bolin, Z. Ying, and G. F. Pedersen, "Spherical coverage characterization of 5G millimeter wave user equipment with 3GPP specifications," *IEEE Access*, vol. 7, pp. 4442–4452, 2019.

[8] S. X. Ta, H. Choo, and I. Park, "Broadband printed-dipole antenna and its arrays for 5G applications," *IEEE Antennas Wireless Propag. Lett.*, vol. 16, pp. 2183–2186, 2017.

[9] I. Syrytsin, S. Zhang, G. F. Pedersen, and A. S. Morris, "Compact quad-mode planar phased array with wideband for 5G mobile terminals," *IEEE Trans. Antennas Propag.*, vol. 66, no. 9, pp. 4648–4657, Sep. 2018.

[10] I.-J. Hwang, B. Ahn, S.-C. Chae, J.-W. Yu, and W.-W. Lee, "Quasi-Yagi antenna array with modified folded dipole driver for mmWave 5G cellular devices," *IEEE Antennas Wireless Propag. Lett.*, vol. 18, no. 5, pp. 971–975, May 2019.

[11] M. Ali, A. O. Watanabe, T.-H. Lin, D. Okamoto, M. R. Pulugurtha, M. M. Tentzeris, and R. R. Tummala, "Package-integrated, wideband power dividing networks and antenna arrays for 28-GHz 5G new radio bands," *IEEE Trans. Compon., Packag., Manuf. Technol.*, vol. 10, no. 9, pp. 1515–1523, Sep. 2020.

[12] A. A. Eldek, A. Z. Elsherbeni, and C. E. Smith, "Wide-band modified printed bow-tie antenna with single and dual polarization for C-and X-band applications," *IEEE Trans. Antennas Propag.*, vol. 53, no. 9, pp. 3067–3072, Sep. 2005.

[13] C. D. Paola, S. Zhang, K. Zhao, Z. Ying, T. Bolin, and G. F. Pedersen, "Wideband beam-switchable 28 GHz quasi-yagi array for mobile devices," *IEEE Trans. Antennas Propag.*, vol. 67, no. 11, pp. 6870–6882, Nov. 2019.

[14] R. Rodriguez-Cano, S. Zhang, K. Zhao, and G. F. Pedersen, "Mm-Wave beam-steerable endfire array embedded in a slotted metal-frame LTE antenna," *IEEE Trans. Antennas Propag.*, vol. 68, no. 5, pp. 3685–3694, May 2020.

[15] S. Zhu, H. Liu, Z. Chen, and P. Wen, "A compact gain-enhanced Vivaldi antenna array with suppressed mutual coupling for 5G mmWave application," *IEEE Antennas Wireless Propag. Lett.*, vol. 17, no. 5, pp. 776–779, May 2018.

[16] P. Liu, X. Zhu, Z. H. Jiang, Y. Zhang, H. Tang, and W. Hong, "A compact single-layer Q-band tapered slot antenna array with phase-shifting inductive windows for endfire patterns," *IEEE Trans. Antennas Propag.*, vol. 67, no. 1, pp. 169–178, Jan. 2019.

[17] D. Chen, K. Wang, W. Zhu, L. Wang, Z. Liu, T. Wang, J. Gao, and S. Zhu, "2–40 GHz dual-band dual-polarised nested Vivaldi antenna," *IET Microw., Antennas Propag.*, vol. 13, no. 2, pp. 163–170, Feb. 2019.

[18] T.-C. Huang, Y.-W. Hsu, and Y.-C. Lin, "End-fire quasi-Yagi antennas with pattern diversity on LTCC technology for 5G mobile communications," in *Proc. IEEE Int. Symp. Radio-Frequency Integr. Technol. (RFIT)*, Taipei, Taiwan, Aug. 2016, pp. 1–3.

[19] Y.-W. Hsu, T.-C. Huang, H.-S. Lin, and Y.-C. Lin, "Dual-polarized quasi Yagi–Uda antennas with endfire radiation for millimeter-wave MIMO terminals," *IEEE Trans. Antennas Propag.*, vol. 65, no. 12, pp. 6282–6289, Dec. 2017.

[20] W. Hong, S.-T. Ko, Y. Lee, and K.-H. Baek, "Compact 28 GHz antenna array with full psolarization flexibility under yaw, pitch, roll motions," in *Proc. 9th Eur. Conf. Antennas Propag. (EuCAP)*, Lisbon, Portugal, Apr. 2015, pp. 1–3.

[21] J. Zhang, K. Zhao, L. Wang, S. Zhang, and G. F. Pedersen, "Dual-polarized phased array with end-fire radiation for 5G handset applications," *IEEE Trans. Antennas Propag.*, vol. 68, no. 4, pp. 3277–3282, Apr. 2020.

[22] R. Rodriguez-Cano, K. Zhao, S. Zhang, and G. F. Pedersen, "Handset frame blockage reduction of 5G mm-Wave phased arrays using hard surface inspired structure," *IEEE Trans. Veh. Technol.*, vol. 69, no. 8, pp. 8132–8139, Aug. 2020.

[23] R. M. Moreno, J. Ala-Laurinaho, A. Khripkov, J. Ilvonen, and V. Viikari, "Dual-polarized mm-Wave endfire antenna for mobile devices," *IEEE Trans. Antennas Propag.*, vol. 68, no. 8, pp. 5924–5934, Aug. 2020.

[24] J. Liu, D. R. Jackson, and Y. Long, "Propagation wavenumbers for half- and full-width microstrip lines in the EH_1 mode," *IEEE Trans. Microw. Theory Techn.*, vol. 59, no. 12, pp. 3005–3012, Dec. 2011.

[25] J. Wang, Y. Li, L. Ge, J. Wang, M. Chen, Z. Zhang, and Z. Li, "Wideband dipole array loaded substrate integrated H-plane horn antenna for millimeter waves," *IEEE Trans. Antennas Propag.*, vol. 65, no. 10, pp. 5211–5219, Oct. 2017.

[26] Q. Wu, J. Hirokawa, J. Yin, C. Yu, H. Wang, and W. Hong, "Millimeter-wave multibeam endfire dual-circularly polarized antenna array for 5G wireless applications," *IEEE Trans. Antennas Propag.*, vol. 66, no. 9, pp. 4930–4935, Sep. 2018.
[27] X. Ruan and C. H. Chan, "An endfire circularly polarized complementary antenna array for 5G applications," *IEEE Trans. Antennas Propag.*, vol. 68, no. 1, pp. 266–274, Jan. 2020.
[28] J. Park, H. Seong, Y. N. Whang, and W. Hong, "Energy-efficient 5G phased arrays incorporating vertically polarized endfire planar folded slot antenna for mmWave mobile terminals," *IEEE Trans. Antennas Propag.*, vol. 68, no. 1, pp. 230–241, Jan. 2020.
[29] Y.-Q. Wen, B.-Z. Wang, and X. Ding, "Planar microstrip endfire antenna with multiport feeding," *IEEE Antennas Wireless Propag. Lett.*, vol. 15, pp. 556–559, 2016.
[30] J. Liu and Q. Xue, "Microstrip magnetic dipole Yagi array antenna with endfire radiation and vertical polarization," *IEEE Trans. Antennas Propag.*, vol. 61, no. 3, pp. 1140–1147, Mar. 2013.

XUE-XIA YANG (Senior Member, IEEE) received the B.S. and M.S. degrees from Lanzhou University, Lanzhou, China, in 1991 and 1994, respectively, and the Ph.D. degree in electromagnetic field and microwave technology from Shanghai University, Shanghai, China, in 2001.

From 1994 to 1998, she was a Teaching Assistant and a Lecturer with Lanzhou University. From2001 to 2008, she was a Lecturer and an Associate Professor with Shanghai University, where she is currently a Professor and the Head of the Antennas and Microwave Research and Development Center. She has authored or coauthored more than 180 technical journal and conference papers. Her current research interests include antennas theory and technology, computational electromagnetics, and microwave power transmission.

Dr. Yang is also a member of the Committee of Antenna Society, China Electronics Institute, and a Senior Member of the China Electronics Institute. She is also a frequent Reviewer for more than ten scientific journals. She is also an Associate Editor of the *Journal of Shanghai University* (Science Edition).

NING-JIE XIE received the B.S. degree from Shanghai University, Shanghai, China, in 2018, where he is currently pursuing the M.S. degree in electromagnetic field and microwave technology.

His current research interest includes 5G antennas.

NAI-DA ZHU received the B.S. and M.S. degrees from Shanghai University, Shanghai, China.

In 2020, he joined Huawei Technologies Company Ltd., Shanghai, where he is currently a Senior Engineer. His current research interests include 5G antennas and mm-wave antennas.

GUO-QIANG HE received the Ph.D. degree (Hons.) in electronic engineering from the Faculty of Engineering Sciences, Vrije Universiteit Brussel, Belgium, in 2019. In 2019, he joined Shanghai University, where he is currently a Senior Lecturer. His current research interests include millimeter wave and terahertz wave sensors, computational electromagnetics, and antenna theory and technique.

MEILING LI (Member, IEEE) was born in Wuhu, China, in 1988. She received the B.S. degree in electronic information engineering from Anhui University, Hefei, China, in 2010, and the Ph.D. degree in electromagnetism field and microwave technology from the University of Science and Technology of China, Hefei, in 2016. She was a Postdoctoral Researcher with the Department of Electronic Engineering and Information Science, University of Science and Technology of China. She is currently a Lecturer with the School of Communication and Information Engineering, Shanghai University. Her research interests include wireless power transfer systems, frequency selected surfaces, absorbing materials and structures, and microwave circuits.

STEVEN GAO (Fellow, IEEE) received the Ph.D. degree in microwave engineering from Shanghai University, Shanghai, China, in 1999. He is currently a Professor and the Chair of the RF and microwave engineering with the University of Kent, Canterbury, U.K. His current research interests include smart antennas, phased arrays, MIMO, satellite antennas, satellite communications, UWB radars, synthetic aperture radars, and mobile communications.